UC Davis
UC Davis Previously Published Works

Title

Retinal organoids derived from rhesus macaque iPSCs undergo accelerated differentiation compared to human stem cells

Permalink

https://escholarship.org/uc/item/194793r2

Journal

Cell Proliferation, 55(4)

ISSN

0960-7722

Authors

Lopez, Antonio Jacobo

Kim, Sangbae

Qian, Xinye

et al.

Publication Date

2022-04-01

DOI

10.1111/cpr.13198

Copyright Information

Peer reviewed

ORIGINAL ARTICLE

Cell
Proliferation WILEY

Retinal organoids derived from rhesus macaque iPSCs undergo accelerated differentiation compared to human stem cells

Antonio Jacobo Lopez[1] | Sangbae Kim[2,3] | Xinye Qian[2,3] | Jeffrey Rogers[2] | J. Timothy Stout[4] | Sara M. Thomasy[1,5] | Anna La Torre[6] | Rui Chen[2,3] | Ala Moshiri[1]

[1]Department of Ophthalmology & Vision Science, School of Medicine, U.C. Davis, Sacramento, California, USA

[2]Human Genome Sequencing Center and Department of Molecular and Human Genetics, Baylor College of Medicine, Houston, Texas, USA

[3]Department of Biochemistry and Molecular Biology, Baylor College of Medicine, Houston, Texas, USA

[4]Department of Ophthalmology, Cullen Eye Institute, Baylor College of Medicine, Houston, Texas, USA

[5]Department of Surgical and Radiological Sciences, School of Veterinary Medicine, University of California, Davis, California, USA

[6]Department of Cell Biology and Human Anatomy, School of Medicine, U.C. Davis, Davis, California, USA

Correspondence
Ala Moshiri, Department of Ophthalmology and Vision Science, School of Medicine, University of California at Davis, Eye Center, 4860 Y. Street, Suite 2400, Sacramento, CA 95817, USA.
Email: amoshiri@ucdavis.edu

Abstract

Purpose: To compare the timing and efficiency of the development of *Macaca mulatta*, a nonhuman primate (NHP), induced pluripotent stem cell (rhiPSC) derived retinal organoids to those derived from human embryonic stem cells (hESCs).

Results: Generation of retinal organoids was achieved from both human and several NHP pluripotent stem cell lines. All rhiPSC lines resulted in retinal differentiation with the formation of optic vesicle-like structures similar to what has been observed in hESC retinal organoids. NHP retinal organoids had laminated structure and were composed of mature retinal cell types including cone and rod photoreceptors. Single-cell RNA sequencing was conducted at two time points; this allowed identification of cell types and developmental trajectory characterization of the developing organoids. Important differences between rhesus and human cells were measured regarding the timing and efficiency of retinal organoid differentiation. While the culture of NHP-derived iPSCs is relatively difficult compared to that of human stem cells, the generation of retinal organoids from NHP iPSCs is feasible and may be less time-consuming due to an intrinsically faster timing of retinal differentiation.

Conclusions: Retinal organoids produced from rhesus monkey iPSCs using established protocols differentiate through the stages of organoid development faster than those derived from human stem cells. The production of NHP retinal organoids may be advantageous to reduce experimental time for basic biology studies in retinogenesis as well as for preclinical trials in NHPs studying retinal allograft transplantation.

1 | INTRODUCTION

High-acuity vision in primates is attributed to the development of the macula lutea (macula)—a region with a high density of cone photoreceptors and specialized circuitry. The center of the macula is the fovea centralis (fovea), which is devoid of retinal vasculature and has a characteristic depression, the foveal pit, which is composed of only tightly packed cone photoreceptors at the exclusion of rods. Many forms of retinal blindness, whether age-related or congenital, ultimately lead to a final common pathway of vision loss due to foveal damage. Inherited retinal disease (IRD), typically associated with single gene mutations, can cause macular dystrophies and cone disorders, which harm the fovea. Age-related macular degeneration (AMD) and related conditions can lead to foveal damage. Retinal vascular disorders such as diabetic retinopathy and occlusive diseases of the retinal vasculature also lead to foveal damage through a combination of macular ischemia and macular edema. The common pathway of most forms of retinal blindness is macular damage and the loss of foveal cones and their supporting cells. Therefore, there is a need for the advancement of cellular regenerative or replacement technologies for patients who have vision loss secondary to foveal cell death. One promising technology is cone photoreceptor transplantation to the macula to restore vision. As terminally differentiated cells, photoreceptors do not have the ability to regenerate. The promise of pluripotent stem cells (PSCs) as a source of photoreceptors through in vitro differentiation has greatly advanced with studies demonstrating the ability to produce consistent and reproducible 3D retinal organoids.[1,2] These results show promise in the possibility for photoreceptor replacement treatments. Transplantation of photoreceptors derived from human pluripotent stem cells have demonstrated promise in rodents,[3–5] felines,[6] and nonhuman primates.[7–9] However, transplantation experiments to the mammalian retina with a macula are relatively few, and successful vision restoration has been limited.[10-12] The translation to clinically relevant treatments relies on the ability to accurately model these therapeutic approaches in a context similar to human patients. While rodents, felids, and canids provide important data on safety and efficacy, they lack true foveal architecture, and therefore, they are not a complete model for the complexity of human macular diseases. It is important to demonstrate the safety and efficacy of these treatments in preclinical trials. Perhaps the best models, we have for preclinical macular studies are nonhuman primates. Nonhuman primates (NHPs) are highly genetically, anatomically, physiologically, and behaviorally similar to humans, and they represent excellent models for translational research when other animal models do not recapitulate the disease of interest. Rhesus macaques (*Macaca mulatta*) are one of the most commonly used NHPs in biomedical research. We have recently described rhesus macaques with inherited retinal disease, which may benefit from transplantation of retinal tissue to restore macular function.[13] Others have also described rhesus macaques with macular abnormalities.[14–16] As the number of NHP models of IRDs expand,

Significance Statement

We demonstrate the generation of retinal organoids from rhesus macaque pluripotent stem cells develops faster than those derived from human stem cells. Usage of rhesus macaque retinal organoids can reduce experimental time for basic biology studies in retinogenesis as well as for preclinical trials in NHPs studying retinal allograft transplantation.

these resources can be useful to study cell transplantation in the context of pre-existing retinal disease. Examples of allogeneic cell transplantation are limited.[17] Exploration of transplantation of allogeneic retinal cells is necessary to overcome the barriers to human clinical studies. Therefore, we have sought to differentiate induced pluripotent stem cells (iPSCs) derived from rhesus monkeys to generate three-dimensional retinal organoids for transplantation into animals with IRDs.

Similar to human stem cells, rhesus macaque iPSCs (rhiPSC) are characteristically indistinguishable from human iPSCs. A previous study using cynomolgus macaque (*Macaca fascicularis)* derived embryonic stem cells demonstrated that the production of retinal cell types from NHP iPSCs is possible using a two-dimensional differentiation protocol.[18] However, while rhiPSCs have been used for the derivation of blood products[19] and cardiac cells,[20–22] little is known about their ability to produce three-dimensional retinal organoids. In this study, we demonstrate the ability of rhiPSCs to produce 3D retinal organoids using a composite established retinal differentiation protocol.[23–25] We characterize the development of rhiPSC-derived 3D retinal organoids and their composition with immunocytochemistry and single-cell next-generation sequencing. To determine the reproducibility of the differentiation protocol, we used three rhesus iPSC lines: two established rhiPSC89[26] and rhiPSC90[27]; and a novel line (from the lab of James Thomson), rhiPSC2431, that is in a defined and xeno-free culture system. Our results demonstrate that rhiPSC-derived retinal organoids follow an abbreviated, but similar development to human iPSC-derived retinal organoids that is consistent with the shorter gestational period of rhesus macaques.

2 | MATERIALS AND METHODS

2.1 | rhiPSC2431 derivation and stem cell culture

Rhesus macaque fibroblasts were generated from skin punches. Using the Neon transfection system pre-set program #16 (1400V, 20 ms, 3 pulses), plasmids used for reprogramming (available from Addgene) were EN2L, ET2K, EM2K, and MIR302, along with EBNA RNA. We transfected 0.5 μg of each plasmid into 4×10^6 fibroblasts per 10-cm vitronectin-coated dish in DMEM/20%FBS/1X

NEAA. After 4–5 days, cells were maintained on vitronectin (5 μg/cm^2) in rhesus iPSC media: Essential 8 Flex Medium (Thermofisher) supplemented with 100-ug/L rhNodal (R&D #3218-ND), 1.94-ug/ml glutathione, 1% chemically defined lipid concentrate (ThermoFisher), 1% GlutaMAX (ThermoFisher), and 1× Pen/Strep Amphotericin B (Lonza, 17-745E). This line was provided by the Thomson lab and assayed for standard pluripotency markers and had a normal karyotype ("Figure S1, hESC and rhiPSC Line Characterization"). rhiPSC89 and rhiPSC90 were maintained on mouse embryonic fibroblasts (MEFs; 50 K/cm^2) (Thermofisher, A34180) in hESC media: 80% DMEM/F12, 20% KOSR, 10-ng/ml bFGF, 1-mM L-glutamine, 0.1-mM B-Me, 1% NEAA, and 1x Pen/Strep Amphotericin B (Lonza, 17-745E). For feeder-free culture, healthy iPSC colonies were manually picked and plated on reduced growth factor Matrigel plates (50 μg/cm^2) in MEF-conditioned hESC media supplemented with bFGF prior to use. Human embryonic stem cell line H9 (WA09, WiCell) was maintained in reduced growth factor Matrigel (50 μg/cm^2) in mTeSR1 plus with 1× Pen/Strep Amphotericin B (Lonza, 17-745E).

2.2 | Retinal differentiation

Spontaneously differentiated cells or iPSC colonies with unhealthy morphology were scraped off before the beginning of differentiation. iPSC colonies were briefly treated with dispase (1-U/ml DMEM/F12) until the edges were slightly curled, at which point the dispase was removed and the colonies were washed with HBSS. Neural induction media (DMEM:F12 1:1, 1% N2 supplement, 1× MEM nonessential amino acids (MEM NEAA), 1× GlutaMAX (Thermo Fisher), and 2-mg/ml heparin (Sigma)) were added, and the iPSC colonies were scraped off and triturated. The fragmented colonies were then plated in low adhesion plates (coated with polyHEMA (8 mg/cm^2)), and corresponding iPSC media were added to achieve 3:1 PSC media/neural induction media (NIM). The embryoid bodies (EBs) were sequentially weaned into neural induction media with 50% media changes replaced by fresh NIM. On day 5, a 50% NIM change was done, and on day 6, the EBs were treated with 1.5-nM recombinant human BMP4 (PeproTech, 10-05ET) in fresh NIM. On day 7, the EBs were plated on reduced growth factor Matrigel (50 EBs/well of a 6-well plate). On day 9 and 12, 50% media was replaced with fresh NIM. On day 15, an additional 50% NIM was added, and the following day, the media was replaced entirely with fresh retinal differentiation media (RDM) (DMEM:F12 3:1, 2% B27 supplement, MEM NEAA, 1× antibiotic, antimycotic (Thermo Fisher), and 1× GlutaMAX)). Retinal differentiation media were changed every other day until day 30. The 3-dimensional structures with lamination-like and optic vesicle-like appearance—retinal organoids—were picked off the plate and resuspended on polyHEMA-coated plates in 3D-RDM (DMEM:F12 3:1, 2% B27 supplement, 1× MEM NEAA, 1× antibiotic, antimycotic, and 1× GlutaMAX with 5% FBS, 100-μM taurine, 1:1000 chemically defined lipid supplement (11905031,

Thermo Fisher)) supplemented with 1 μM of all-trans-retinoic acid until day 100. 3D-RDM either with or without RA supplementation was changed twice per week.

2.3 | Immunocytochemistry

Retinal organoids were fixed with 4% PFA on ice for 20 min and then washed three times with DPBS. The retinal organoids were then equilibrated in 15% sucrose and 30% sucrose until they sunk. The retinal organoids were then flash frozen in dry ice-ethanol bath in Tissue-Plus OCT compound. Subsequently, the blocks were sectioned at 10 μm and blocked in blocking solution (4% BSA and 0.5% Triton X-100 in PBS) for an hour at room temperature. Primary antibodies were then incubated at 4°C overnight. Excess primary antibody was washed off with three washes of PBS. Alexa Fluor-conjugated secondary antibodies matching the primary antibody host were incubated for an hour followed by 5-min incubation in DAPI. The slides were then washed three times, one minute per wash. Finally, the slides were cover slipped with FluorSave Reagent (Millipore, 345789). A table of primary and secondary antibodies is included in Figure S2. The samples were then imaged using an Olympus FluoView FV1000 spectral confocal microscope.

2.4 | TEM

Organoids were fixed in 3% glutaraldehyde and 1% paraformaldehyde in 0.08-M sodium cacodylate buffer (all from Electron Microscopy Sciences) overnight with gentle rocking at 4°C, washed with 0.1-M cacodylate buffer, and postfixed in 1% osmium tetroxide for 2 h at RT. The organoids were then dehydrated in a graded ethanol series, further dehydrated in propylene oxide and embedded in Epon epoxy resin. Semithin (1 μm) and ultrathin sections were cut with a Leica EM UC6 ultramicrotome and the latter were collected on pioloform-coated (Ted Pella, 19244) one-hole slot grids. Sections were contrasted with Reynolds lead citrate and 8% uranyl acetate in 50% ethanol and imaged on a Philips CM120 electron microscope equipped with an AMT BioSprint side-mounted digital camera and AMT Capture Engine software.

2.5 | Single-cell sequencing and data analysis

Single-cell cDNA library preparation and sequencing were performed following manufacturer's protocols (10× genomics). Single-cell suspension at 1000 cells/μl in PBS were loaded on a chromium controller to generate single-cell GEMS (Gel Beads-In-EMulsions). The scRNA-Seq library was prepared with chromium single-cell 3' reagent kit v3 (10× Genomics). Cell Ranger software v3.1 (https://www.10xgenomics.com) with default settings was used for alignment, barcode assignment, and UMI counting of the raw sequencing data with genome reference hg19. After generating UMI count

profile, we applied Seurat 4.0 (https://satijalab.org/seurat) for quality control and downstream analysis.

For quality control, we excluded genes detected in less than 3 cells, and cells were filtered out if UMI counts are less than bottom 3% and greater than top 1% of total quantile. We removed cell-cycle effects by regressing out cell-cycle scores during data scaling using of all signals associated with cell cycle using "CellCycleScoring" function in Seurat. Next, a global-scaling normalization method 'LogNormalize' in Seurat was employed to normalize the gene expression measurements for each cell by the total expression, then the result is multiplied by a scale factor (10,000 by default) and log-transformed. We selected variable genes and computed principle components for dimensional reduction of UMAP with default parameters of Seurat. Next, we performed the clustering using 'FindClusters' in Seurat to identify sub-cell-type clusters. Top 20 principle components were used with 0.1 resolution, and the sub-populations of corneal cells are visualized using UMAP. To identify differentially expressed marker genes in each cluster, we used the 'FindAllMarkers' function based on the Wilcoxon rank-sum test in Seurat with default parameters, and then, cell types were assigned using known cell-type markers. Top 10 DEGs were visualized with a heatmap using Seurat. We also performed cell-cycle analysis to estimate cell-cycle status of each cell using cell-cycle markers using Seurat.

For trajectory analysis, we used Monocle 3 to infer the cell differentiation trajectories with default parameters (https://cole-trapnell-lab.github.io/monocle3/). This method places the cells along a trajectory corresponding to a biological process (in our case, cell differentiation) by taking advantage of an individual cell's asynchronous progression under an unsupervised framework.

3 | RESULTS

3.1 | Rhesus iPSCs differentiate into 3D retinal organoids

In this study, we differentiated three different rhiPSC lines using a stepwise retinal differentiation protocol to generate retinal organoids (Figure 1A). Undifferentiated stem cell colonies were cultured in nonadherent conditions to generate embryoid bodies (EBs), which were cultured in neural induction media (NIM) for 7 days. Next, the EBs were plated onto Matrigel-coated plates and grown in 2D from day 7 to 30 at which time, the regions of the culture displaying retinal morphology were selected, lifted, and grown in nonadherent 3D conditions (Figure 1B). The morphology of the rhiPSC-derived cultures developing retinal tissue was very similar to that observed in H9 hESCs. Following the criteria proposed in Capowski et al.[28] we binned retinal organoids into three stages: stage 1, retinal organoids displaying phase bright appearance; stage 2, retinal organoids displaying phase dark appearance; and stage 3 retinal organoids displaying outer segment protrusions (Figure 1C).

During the 2D-retinal differentiation protocol, we noticed that the self-organizing optic vesicle-like structures (OVs) developed earlier and were well formed as early as day 20 (Figure 1B, Day 20). OV formation was not mutually exclusive to formation of neural rosettes[3] or horseshoe-like structures described by others.[29] OVs continued to develop until day 30, at which point they were manually selected from the plate and resuspended in 3D-RDM media supplemented with retinoic acid (RA) until day 100. Thereafter, the retinal organoids were cultured in 3D-RDM until analysis.

3.2 | Rhesus retinal organoids undergo appropriate morphological and structural differentiation

Stage 1 retinal organoid sections were examined (day 44) with light microscopy (Figure 2A). At this stage, some organoids had a variable number of cells in the inner layers. Smaller organoids usually had a higher density of cells in their core (Figure 2A') while larger organoids, as they transition to stage 2, developed a hollow core. There was further loss of the inner cells as retinal organoids developed to stage 3. The outer aspect of rhesus retinal organoids had discrete shape and boundaries facing their environment, while the internal boundary was poorly defined (Figure 2A, 2A'). Stage 2 and 3 organoids were similar to one another in that they had a loss of inner cells; however, we also observed a thickening of the outer layer. Similar to hiPSC-derived retinal organoids, stage 3 was defined with the development of outer segment-like morphology (Figure 1C'). To further elucidate whether the structures observed were photoreceptor segments, stage 3 retinal organoids (125 days) were analyzed through transmission electron microscopy (Figure 2B,B',C,C'). The photoreceptor protrusions were composed mostly of inner segment-like structures (Figure 2B,B', IS) that were mitochondria-rich (2B', MT). There was also a presence of a loose outer limiting membrane (Figure 2B,B', OLM). Outer segments (OS) and connecting cilium structures were also observed (Figure 2C, OS and Figure 2C' CC, respectively). These ultrastructural findings demonstrate that stage 3 retinal organoids can develop photoreceptor structures similar to those observed in human retinal organoids.

3.3 | Rhesus retinal organoids express retinal cell-type–specific markers

Stage 1 retinal organoids are composed of neural retinal progenitors, retinal ganglion cells and early photoreceptors. Immunocytochemistry of stage 1 retinal organoids demonstrated an abundance of eye field transcription factors and retinal progenitor markers such as PAX6, RX, LHX2, OTX2, and CHX10 (Figure 3B,C,F,I,N, respectively). Counterstaining with DAPI is also shown (Figure 3A,E,H,L,P,T). In human retinal organoids, early photoreceptors localized to the outer perimeter. Cells expressing both OTX2 and Blimp1 (Figure 3 H–K) are committed to photoreceptor fates.[30] By using these fate restriction markers, we were

FIGURE 1 Schematic diagram and phase microscopy of rhesus retinal differentiation protocol. (A) Schematic diagram of the differentiation protocol used to produce 3D-rhesus retinal organoids. (B) Representative phase images of the differentiation protocol before plating on Matrigel-coated plates (day 7), rosette formation (day 14), and the development of optical vesicle-like structures (day 20 and day 30). (C) Representative phase images of rhesus retinal organoids in suspension (stage 1, 44 days; stage 2, 80 days; and stage 3, 105 days (rhipsc89 and 90), and 125 days (rhiPSC 2431). (C') High-magnification image of the marked area demonstrating the hair-like extrusions on the perimeter of the retinal organoids
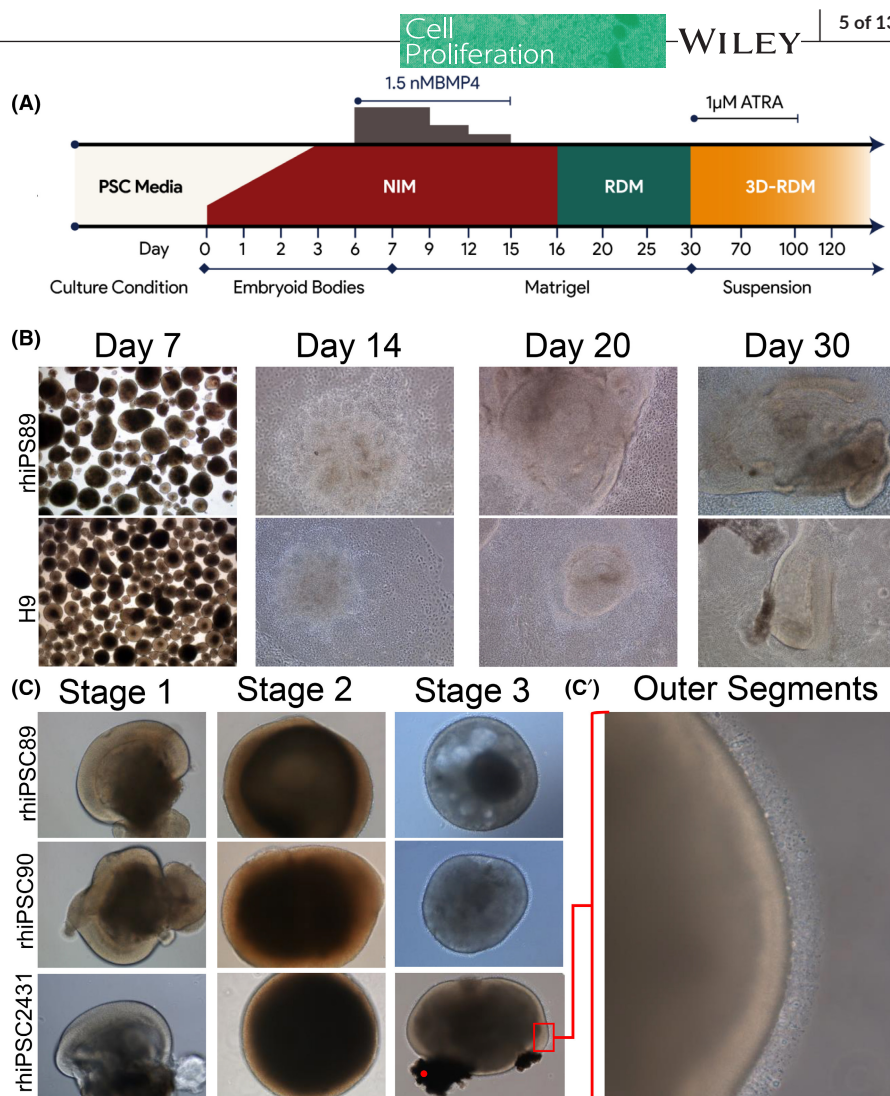
able to determine that as early as stage 1, early photoreceptors (presumably cones) were primarily localized to the outer perimeter of the organoid. Similarly, we also observed double-positive cells expressing both recoverin and CRX, further indicative of photoreceptors precursors (Figure 3P–S). CRX-/recoverin-positive cells primarily resided in the outer perimeter of the organoids, while other cells lacking these markers resided in the inner layers. However, they were not restricted to the innermost aspect of the organoids. Furthermore, markers of the beginnings of bipolar cell fate specification[30] (OTX2+/CHX10+) were also discernible at this stage (Figure 3L–O), though most if not all of the CHX10+ nuclei at this stage likely represent progenitors. Retinal ganglion cells (RGCs, BRN3+, and TUJ1+, Figure 3T–W) were abundant lining primarily the internal perimeter of the organoids. The nuclei of retinal ganglions cells were primarily found in the inner core of the organoid, while their processes could span to the outer aspect of the organoids. The relative localization of photoreceptors and RGCs corresponds to the lamination seen in the retina in vivo. While there was not a clear separation between neural retinal progenitors and retinal ganglion cells, the distinct localization of RGC nuclei suggests the possible formation of inner retinal lamination. Lower power images are shown in Figure S3.

Stage 2 retinal organoids are composed of high populations of photoreceptor precursors. During stage 2, the retinal organoids had increased CRX- and recoverin-positive cells (Figure 4A-D) as well as OTX2 (Figure 4E-G), indicating differentiation of photoreceptors. For all these markers, photoreceptors tended to occupy the outer aspect of the organoid, but some were at times observed on the inner portion of the organoid. The development of an outer nuclear layer (ONL) could be seen advancing at this stage with a light nuclear stratification (Figure 4E'-G', dashed line). The ONL was 3–5 nuclei in thickness at this stage. Outer segments were not present, but the outer perimeter of the organoid was clearly defined. The internal composition of the stage 2 organoids, while not hollow like in stage 1, was disorganized. By stage 2, RGCs were no longer present (Figure 4H-K). We did not observe BRN3-positive cells (Figure 4I). However, there was some TUJ1-positive signal (Figure 4J,K) that we presumed to be neurites of degenerating RGCs that no longer labeled with BRN3 as the nuclei were probably apoptotic. Lower power images are shown in Figure S4.

Stage 3 retinal organoids have developed outer segment-like structures, which appear as translucent hair-like protrusions covering the majority of the retinal organoids. Similar to what has been observed in human retinal organoids, there was a presence
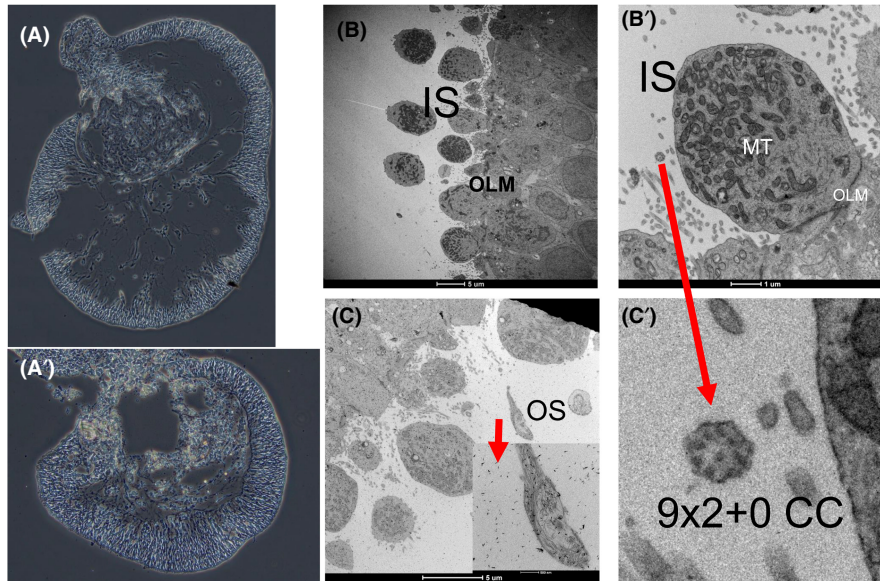
FIGURE 2 Light microscopy and transmission electron microscopy structural analysis of rhesus retinal organoids. (A) Phase image of a 44-day old rhesus retinal organoid. The perimeter of the retinal organoids were cell dense, while internally, cells were sparse. (A') Phase image of a smaller 44-day-old rhesus retinal organoid that contained more internal cells. (B) Transmission electron microscopy of the perimeter of stage 3 rhesus retinal organoids (125 days) demonstrating inner segments (IS), an outer limiting membrane (OLM) (B') Inner segments were mitochondria (MT) rich. (C) Outer segment (OS). (C') Magnification of B' demonstrating a $9 \times 2 + 0$ structure of connecting cilia (CC)

of darkly pigmented cells consistent with RPE (Figure 1C, Stage3 of rhiPSC2431, red dot). Staining for ARR3 (cone arrestin) in Stage 3 (Figure 5B) demonstrated photoreceptors in the outer perimeter of these organoids. The development of these Stage 3 characteristics was observed regularly at 105 days, while they were not consistently observed in human retinal organoids regularly until about 200 days. During stage 3, we observed S-opsin-, M/L opsin-, and rhodopsin-positive cells (Figure 5C,H,D, respectively) localized to the outer segment rather than the cell body, indicating appropriate trafficking of phototransduction machinery in differentiating photoreceptors. While earlier stages had faint separation in the ONL and INL, by this stage, we saw that there was a clearer delineation of retinal layers (Figure 5K). The outer layer of stage 3 organoids was composed of an outermost layer of 1–2 cone photoreceptor nuclei (Figure 5G–J, CRX-positive, M/L opsin-positive, NRL-negative cells) stacked on a 1–3 rod photoreceptor nuclei layer (Figure 5G–J, NRL-positive, CRX-positive). Cone photoreceptors displayed outer segments that were ARL13B-positive (Figure 5R) and have pedicles that were localized with CTBP2 (Figure 5S). The inner layer was composed of both CHX10-positive bipolar cells (Figure 5N) and SOX9-positive Muller Glia (Figure 5X). The inner layer was somewhat less stratified and organized than the outer layer of the organoid at this stage. As we observed in stage 2, there were no longer any retinal ganglion cells (BRN3/TUJ11 double-positive cells), but some TUJ1-positive neurites persisted (Figure 5U–Y). Similarly, photoreceptors previously observed in the inner aspect of the organoid, likely representing newly born photoreceptors undergoing radial somal migration, were for the most part absent. However, occasionally, they arranged themselves into rosettes with outer segments pointing toward the center (Figure 5P'-T'). Lower power images are shown in Figure S5.

3.4 | Single-cell RNA-seq showed stage-appropriate retinal cell types in rhesus retinal organoids

In order to determine the cell types being produced in rhesus retinal organoids, we used single-cell RNA sequencing (scRNA-seq). We chose retinal organoids from early stage 2 and stage 3 for these experiments in order to capture the peaks of differentiation of early and late retinal cell types. The studies of retinal organoids at these stages demonstrated heterogeneity in retinal cell types in the monkey retinal organoids at both of the time points (67 days and 173 days). A combined total of 23,218 cells were captured and sequenced using 10× Genomics' single-cell scRNA-seq technology. We aligned the raw sequence data, performed quality control, and normalized the transcriptional profiles using the manufacturer's Cell Ranger software. The profile data of 19,894 single cells (D67; 11,103 cells and D173; 8,791 cells) were obtained and visualized. A uniform manifold approximation and projection (UMAP) plot was used for the unbiased clustering of single cells from retinal organoids from both time points based on retinal cell-type–specific markers (Figure 6A). Combined data after merging and processing two raw count matrices using Seurat are shown (Figure 6B). The proportion of cell populations in clusters (Figure 6C) of the combined data were tabulated, as were dot plots, showing the expression level of known markers for specific retinal cell types (Figure 6D). These experiments confirmed the presence of early and late retinal progenitor populations, RGCs, and amacrine cells in early stage 2 organoids. These data also demonstrate the presence of cone and rod photoreceptors (ratio of 0.49 cone to rod), Muller glia, ON- and OFF-bipolar cells, amacrine cells (AC), and horizontal cells in stage 3 retinal organoids, with an absence of retinal ganglion cells. Cell-cycle scoring of retinal

FIGURE 3 ICC of Stage 1 (44 days): Retinal organoids are composed of neural retinal progenitors, retinal ganglion cells, and early photoreceptors. (A, E, H, L, P and T) DAPI counterstain. (B, C, F, I, M and N) Retinal organoids expressed eye field transcription factors Pax6, Rx, Lhx2, Otx2, and Chx10, respectively. (H–K) Retinal organoids contained Otx2+/Blimp1+ cells, markers of early photoreceptor fate restriction. Similarly, (L–O) showed a few Otx2+/Chx10+ cells, which may be early bipolar-fated cells, though most if not all of the CHX10+ nuclei at this stage likely represent progenitors. (P–S) An early population of developing photoreceptors (recoverin+/CRX+) was also present. (T–W) Tuj1+/Brn3+ retinal ganglion cells were present on the inner aspect of the organoids. All scale bars are 100 μm
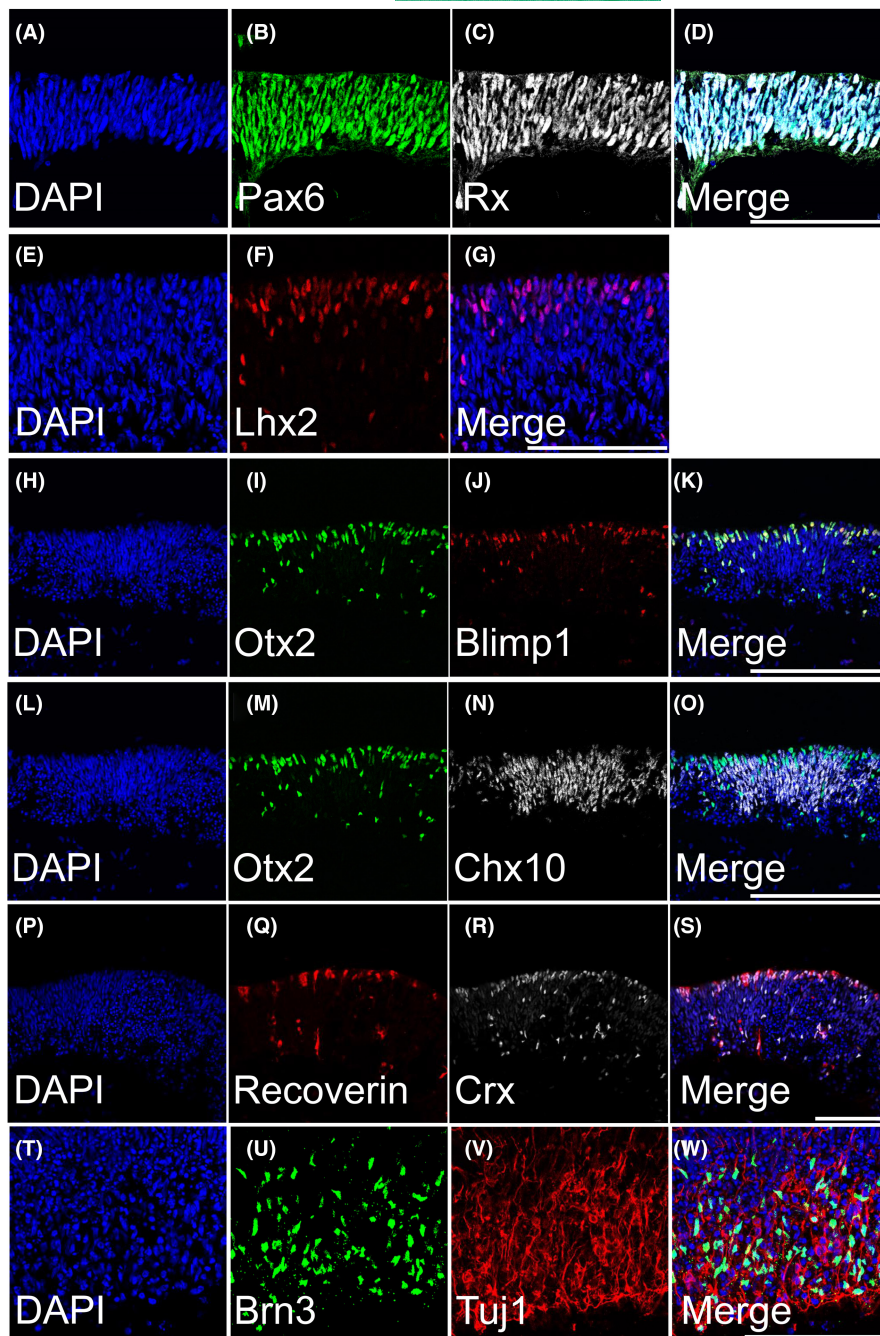

organoids (Figure S6) as well as violin and feature plots of known retinal cell-type–specific markers (Figure S7) was also assessed.

3.5 | Rhesus stem cells differentiate precociously and less efficiently compared with human stem cells

We used light microscopy to systematically assign morphological staging levels to retinal organoids based on criteria defined by Capowski et al.[28] In general, stage 1 retinal organoids developed into stage 2 after a few weeks and stage 3 developed as early as 105 days. The three rhesus iPSC lines used in this study generally showed similar characteristics in both morphology and timing of differentiation despite somewhat different culturing systems required

to maintain them prior to entering the differentiation process. When compared to the H9 human stem cells used for retinal differentiation, we observed rhesus cells passed through the three stages of organoid maturation more quickly than H9 cells (Figure 7A). At day 45, rhesus iPSCs and H9 cells could be seen in stage 1 or 2, and by day 80, most rhesus and human organoids had achieved stage 2 morphology. However, by day 120, virtually all rhesus organoids had developed the outer segment-like projections characteristic of stage 3, while this was never observed in human organoids at this time point. Several rhesus organoids reached stage 3 morphology by day 105. Even at day 150, only a small fraction (~10%) of human organoids had reached stage 3, which was more commonly attained by day 200. These findings are consistent with the 40% shorter gestational age of the rhesus macaque compared to that of
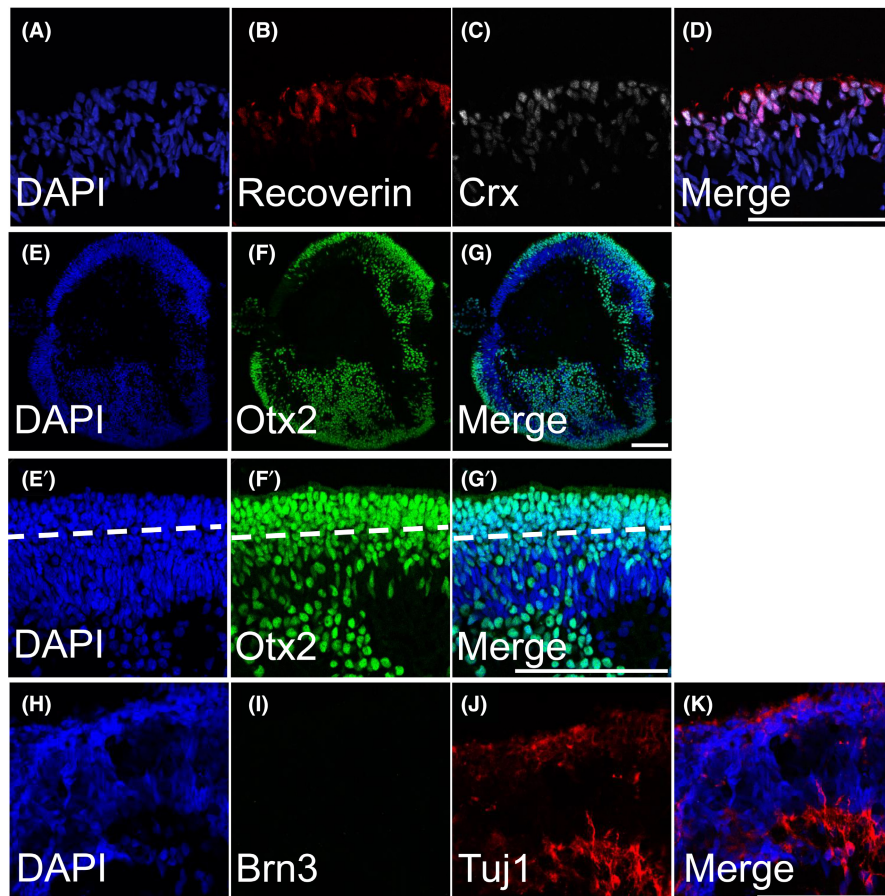
FIGURE 4 ICC of Stage 2 (80 days): Stage 2 retinal organoids are composed of differentiating photoreceptors and have lost retinal ganglion cells. (A, E, E' and H) DAPI counterstain. (A–D) Stage 2 retinal organoids had high numbers of developing photoreceptors (CRX+/recoverin+) and photoreceptors progenitors (Otx2+) (E–G). While a high density of photoreceptors were localized to the outer perimeter, there were also a substantial number of unorganized photoreceptors that were localized in the inner portion of the retinal organoids. (E'–G') Higher magnification images of panels E–G, with a dashed line indicating a developing IPL. (H–K) Stage 2 retinal organoids were devoid of Brn3+ cells and had sparse Tuj1 staining. All scale bars are 100 μm

human. Despite the precocious passage through the stages of retinal organoid differentiation relative to human, rhesus iPSC-derived cells underwent self-organization into retinal morphology much less frequently in our protocol. Ninety percent of our differentiation experiments using H9 cells resulted in at least one retinal organoid and were considered successful experiments. However, in rhesus iPSCs, the vast majority of differentiation experiments yielded no retinal organoids, with only 1.9%–4.7% of experiments successfully yielding at least one retinal organoid (Figure 7B). Similarly, the proportion of embryoid bodies, which adopted retinal morphology was 26.1% in human stem cells, but only 1.4%–4.7% in rhesus iPSCs (Figure 7C). We attempted to modify the differentiation protocol, in particular by abbreviating the early steps to better suit the intrinsic timing of rhesus macaque iPSC differentiation (Figure S8). However, our attempts did not yield better results.

4 | DISCUSSION

Retinal research in NHPs is of particular importance due to the presence of macular and foveal structure, which is required for high-acuity vision. The relevance of macular studies to human disease and translation to clinical trials can hardly be overstated. Studies of cell-based therapies ultimately need to be evaluated in the context of allograft transplantation, since human trials will almost certainly involve the use of human cells. Therefore, optimizing the process of cell-based treatments in preclinical models will benefit from using cells of the same species. The value of studying rhesus retinal organoids is that the cells introduced to the NHP host are from the same species. The learnings from this line of experimentation can later be evaluated in the context of human studies once optimized in NHPs. In addition to translational studies, rhesus retinal organoids are useful

FIGURE 5 ICC Analysis of Stage 3 rhesus retinal organoids demonstrate highly developed photoreceptors, Muller glia, and bipolar cells. (A, F, K, P, P' and U) DAPI counterstain. Stage 3 retinal organoids (105 days) were analyzed by ICC. Retinal organoids at 105 days displayed localization of photopigment in the outer segment rather than in the cell body. (B) Cone arrestin was diffused throughout the body of cone photoreceptors unlike photopigments (C) S-opsin, (D) rhodopsin, and (H) M/L opsins, which were more densely localized to the outer segment. (G and I) Nuclear labeling of rod photoreceptors (NRL) and all photoreceptors (CRX) showed that there was a layer of 1–2 cone photoreceptor nuclei stacked on top a layer of 1–3 rod nuclei layer. (K) At this stage, there was a clear divide between two nuclear layers. The inner layer was more loosely packed than the outer layer. The inner cell layer contained both (N) bipolar cells (CHX10) and (X) Muller glia (SOX9). (R) Outer segment cilia were present (ARL13B). (S) CTBP2 colocalized to cone arrestin pedicles. (Q'–T') Most of the time, inner photoreceptors were disorganized, but there were occasional instances where the photoreceptors arranged in rosettes. Photoreceptors seemed to organize themselves so that their outer segments (Q') were at the center of the rosette rather than the pedicle. (V–W) No Brn3+ RGC nuclei were seen, though some Tuj1 signal persisted. All scale bars are 100 μm except for A–J, which are 10 μm
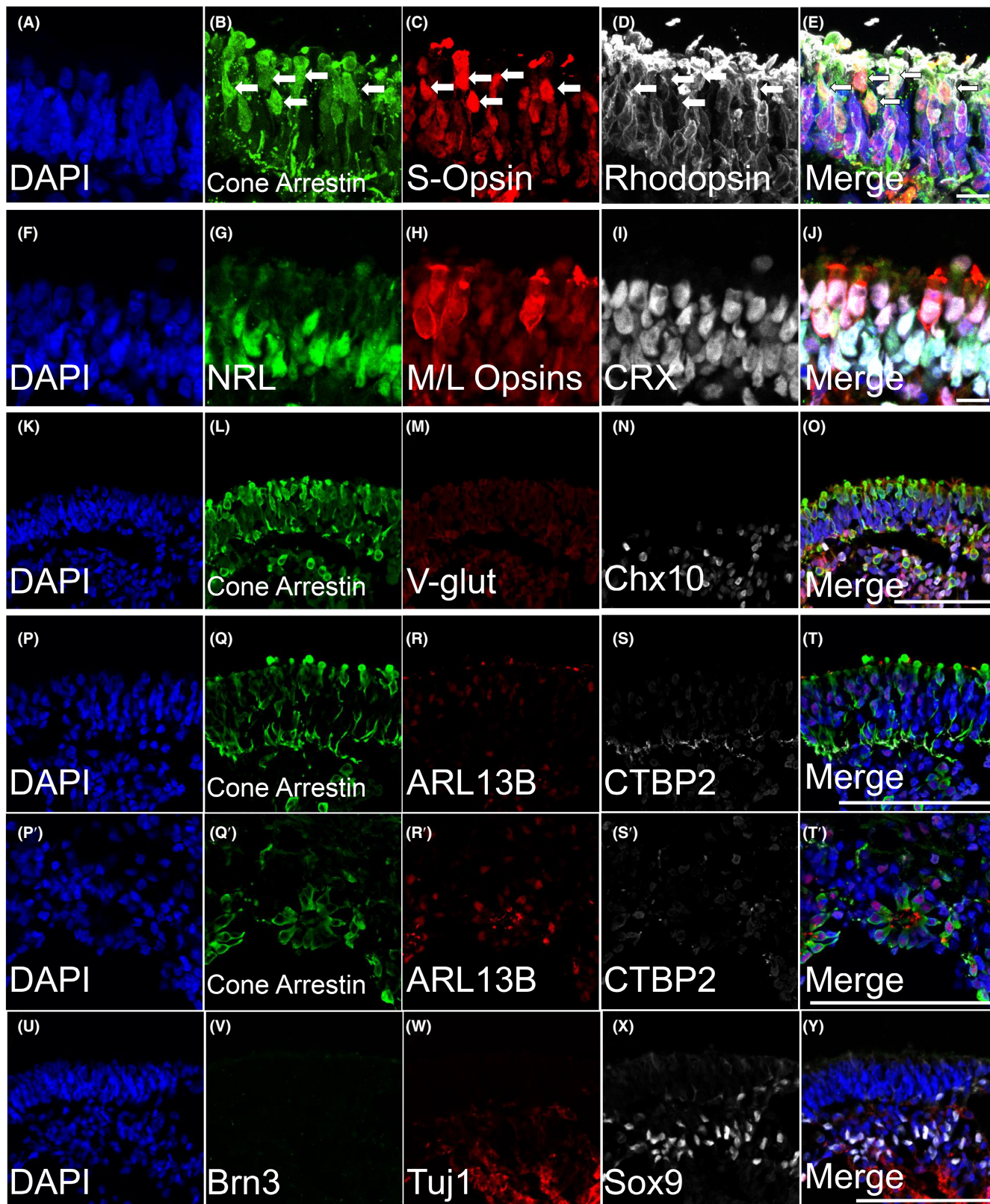
for studying macular developmental biology and patterning, including cell fate specification of early retinal cell types, which make up foveal architecture. The more rapid differentiation quantified in this study emphasizes the potential efficiency of using rhesus iPSCs compared to that of human stem cells for developmental experiments.

The gestational time in humans (280 days, ~40 weeks) is 40% longer than in rhesus macaques (166.5 days, ~23 weeks).[31] Our hypothesis, based on the difference in gestational age, was that development of retinal organoids and their acquisition of outer segments may occur in an accelerated fashion resulting in
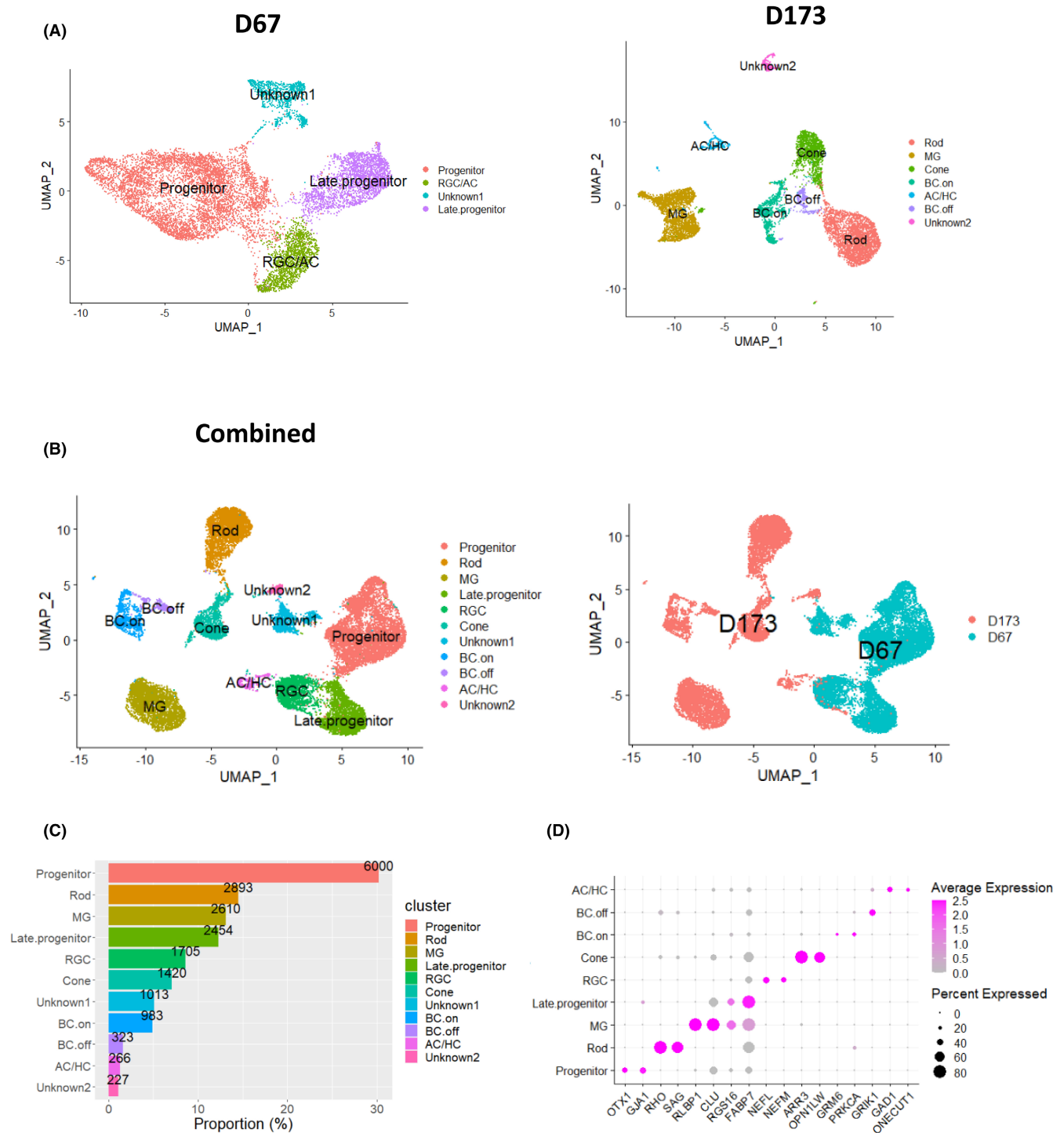
FIGURE 6 scRNA-seq revealed the heterogeneous cell types in NHP retinal organoids at two different time points (67 days and 173 days). Total 23,218 cells were captured and sequenced using 10× Genomics' single-cell RNA-seq (scRNA-seq) technology. After aligning raw sequence data and quality control and normalization of transcriptional profiles using Cell Ranger software v3.1 (10× genomics) with default settings and Seurat package (V4.0.1), the profile data of 19,894 single cells were obtained and visualized. (A) Uniform manifold approximation and projection (UMAP) plot were used for the unbiased clustering of single cells from retinal organoids with two different time points (D67; 11,103 cells and D173; 8,791 cells) based on retinal cell-specific markers. Left panel represents output from D67 and right ones for D173. (B) UMAP of the combined data after merging and processing two raw count matrices using Seurat. The UMAPs are visualized by cell type in the left and by each data set in the right. (C) Proportion of cell populations in clusters of the combined data. Numbers on bar indicate the number of cells. (D) Dot plots show the expression level of known cell-type markers for specific cell types: OTX1 and GJA1 for progenitor, RHO and SAG for Rod, RLBP1 and CLU for Muller glia (MG), RGS16, and FABP7 for Late progenitor, NEFM and NEFL for RGC (Retinal ganglion cell), ARR3 and OPN1LW for Cone, GRM6 and PRKCA for ON Bipolar (BC.on), GRIK1 for OFF Bipolar (BC.off), GAD1 for Amacrine cell (AC), ONECUT1 for horizontal cell (HC) on the right panel. Cell types were not assigned for Unknown1 and 2 clusters

FIGURE 7 Rhesus iPSC lines differentiated precociously but less efficiently than human stem cell derived retinal organoids. (A) Both rhesus and human stem cells generated a significant proportion of stage 1 and 2 retinal organoids at early time points. However, stage 3 morphology marked by outer segment-like projections were seen in the majority of rhesus organoids at day 120 but were never observed in human organoids at this time point. By day 150, approximately 10% of human organoids had achieved stage 3 morphology. (B) The vast majority of differentiation experiments yielded retinal morphology when H9 cells were used, while under 5% of experiments with rhesus cells ever yielded retinal organoids. (C) The proportion of embryoid bodies, which adopted retinal morphology was also less than 5% in rhesus cells, while 26.1% of H9 embryoid bodies formed retinal organoids
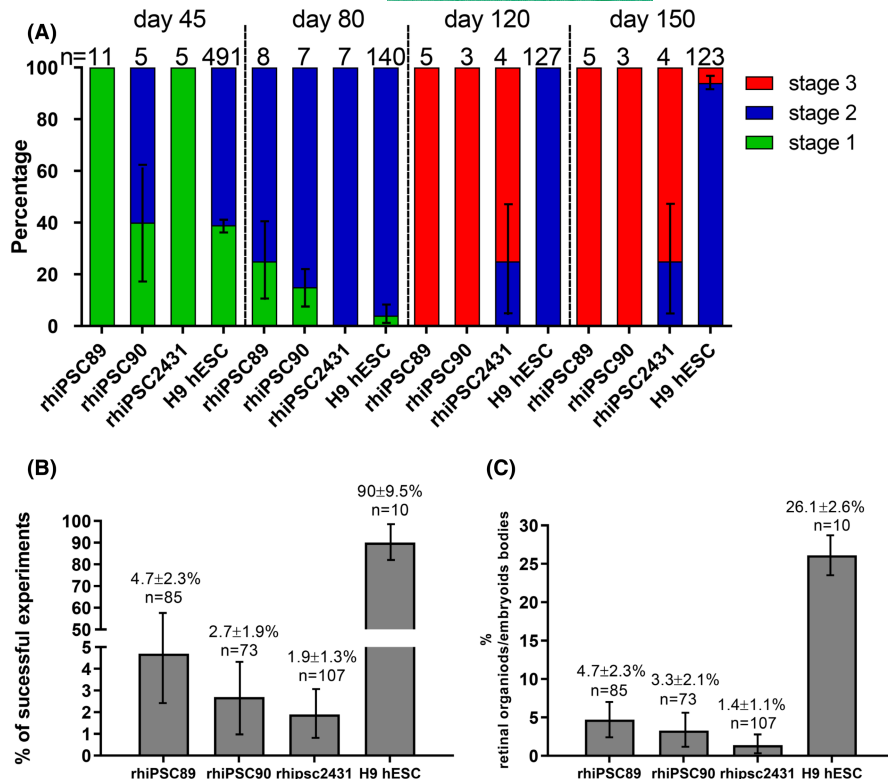
relatively precocious differentiation when compared to human iPSC-derived retinal organoids. Our earliest observation of outer segments was on day 105 in rhesus and day 150 in human organoids. This represents attainment of stage 3 characteristics 30% sooner in rhesus retinal organoids, which roughly corresponds to the difference in gestational age between these species, especially if taking into account that humans are generally considered full term at 37 weeks.[32] We have also empirically observed that when embryoid bodies are plated on Matrigel for the self-organization into OVs, rhesus OVs organize slightly sooner, albeit less frequently, than human counterparts. At day 20, clear OVs were visible, while human OVs are just starting to form by this time. As demonstrated in our ICC of each stage, in rhesus macaque-derived retinal organoids, there is greater overlap of photoreceptor markers, which could not be segregated purely by light microscopy-based binning. This is especially true for stage 1 retinal organoids that demonstrate early photoreceptor markers typically seen in stage 2 human retinal organoids. The formation of an outer nuclear layer, which coincides with the loss of retinal ganglion cells are events that occur in stage 2. Studies that seek to enrich for retinal ganglion cells might focus on stage 1 to quantify RGC enrichment or to test the efficacy of neuroprotective interventions.

Rhesus retinal organoids have the advantage of using a primate cell culture model with much closer genetic and macular structural similarity to humans when compared to mouse retinal organoids. In addition, the development of rhesus retinal organoids is faster in cell culture than humans, which may be advantageous to study mechanistic developmental processes specific to primates. By reducing the time to obtain highly differentiated stage 3 retinal characteristics by

30%–40% over human retinal organoids, there may be an advantage of both time to experimental results and reagent expenses. However, given the low efficiency of rhesus organoid production, the differentiation protocol must be optimized for species differences in order to fully capitalize on these advantages.

Various studies have used NHPs as a clinical model for retinal cell replacement, with limited success. A contributing factor might be the use of human cells in NHPs. Interspecies differences may be circumvented by using NHP-derived retinal cells for allogeneic or even autologous transplants. This may be particularly important for preclinal studies where both safety and efficacy of cellular products delivered to the macula would be helpful to demonstrate in NHPs in advance of human clinical trials.

Other uses for rhesus retinal organoids include studies aimed at understanding the developmental processes of the primate retina. There are many questions regarding the genetic patterning of the macula, which could be addressed using rhiPSCs as they proceed through the differentiation process faster than human counterparts. Similar questions about cell fate determination of cone photoreceptor subtypes could be addressed. Translational applications of rhesus retinal organoids may help determine whether allogenic transplantation of cells to the retina improves integration of donor cells into the host, since human cells may have limited potential to functionally integrate.

5 | CONCLUSION AND/OR SUMMARY

Here, we have demonstrated that the derivation of retinal organoids from rhesus macaques is possible and that they closely

resemble native retinal tissue. Like what has been observed in human-derived retinal organoids, there is high variability between differentiation experiments within the same stem cell lines and across different lines (regardless of iPSCs or hESCs). In this study, we compared three different lines, from which we could obtain retinal organoids, though rhiPSC89 and rhiPSC90 lines produced more retinal organoids that reached stage 3 compared with rhiPSC2431. Rhesus iPSC lines are more difficult to culture and may require feeder layers of MEFs since they have a tendency to differentiate prematurely in their absence. The difficulty in maintaining them may outweigh the potential savings in the shorter retinal differentiation time. Optimization of a feeder-free system that is similar to that of human PSCs in an mTESR1 system would be advantageous. Another consideration to take into account is that the differentiation protocol will have to be modified to increase the efficiency of retinal organoid production from rhesus iPSCs. Optimization of the retinal differentiation protocol for rhesus iPSCs is the subject of continued research.

CONFLICT OF INTEREST
The authors declare no conflicts of interest related to this study.

AUTHOR CONTRIBUTIONS
Antonio Jacobo Lopez was involved in conception and design, collection and/or assembly of data, data analysis and interpretation, and manuscript writing. Sangbae Kim was involved in collection and/or assembly of data, data analysis and interpretation, and manuscript writing. Xinye Qian was involved in collection and/or assembly of data, data analysis and interpretation. Jeffrey Rogers, J. Timothy Stout, Sara M. Thomasy, and Anna La Torre were involved in final approval of the manuscript. Rui Chen was involved in conception and design, financial support, provision of study material, collection and/or assembly of data, data analysis and interpretation, and final approval of the manuscript. Ala Moshiri was involved in conception and design, financial support, provision of study material, collection and/or assembly of data, data analysis and interpretation, manuscript writing, and final approval of the manuscript.

DATA AVAILABILITY STATEMENT
The data that supports the findings of this study are available in the supplementary material of this article.

ORCID
Antonio Jacobo Lopez https://orcid.org/0000-0003-2391-3593
Ala Moshiri https://orcid.org/0000-0002-4277-8094

REFERENCES
1. Nakano T, Ando S, Takata N, et al. Self-formation of optic cups and storable stratified neural retina from human ESCs. *Cell Stem Cell.* 2012;10(6):771-785.
2. Eiraku M, Takata N, Ishibashi H, et al. Self-organizing optic-cup morphogenesis in three-dimensional culture. *Nature.* 2011;472(7341):51-56.
3. Lamba DA, Gust J, Reh TA. Transplantation of human embryonic stem cell-derived photoreceptors restores some visual function in Crx-deficient mice. *Cell Stem Cell.* 2009;4(1):73-79.
4. Reh TA, Lamba D, Gust J. Directing human embryonic stem cells to a retinal fate. In: Ding S, ed. *Cellular Programming and Reprogramming: Methods and Protocols.* Humana Press; 2010:139-153.
5. Lamba DA, McUsic A, Hirata RK, Wang P-R, Russell D, Reh TA. Generation, purification and transplantation of photoreceptors derived from human induced pluripotent stem cells. *PLoS One.* 2010;5(1):e8763.
6. Singh RK, Occelli LM, Binette F, Petersen-Jones SM, Nasonkin IO. Transplantation of human embryonic stem cell-derived retinal tissue in the subretinal space of the cat eye. *Stem Cells Dev.* 2019;28(17):1151-1166.
7. Shirai H, Mandai M, Matsushita K, et al. Transplantation of human embryonic stem cell-derived retinal tissue in two primate models of retinal degeneration. *Proc Natl Acad Sci.* 2016;113(1):E81-E90.
8. Chao JR, Lamba DA, Klesert TR, et al. Transplantation of human embryonic stem cell-derived retinal cells into the subretinal space of a non-human primate. *Transl vis Sci Technol.* 2017;6(3):4.
9. Aboualizadeh E, Phillips MJ, McGregor JE, et al. Imaging transplanted photoreceptors in living nonhuman primates with single-cell resolution. *Stem Cell Reports.* 2020;15(2):482-497.
10. McGill TJ, Stoddard J, Renner LM, et al. Allogeneic iPSC-derived RPE cell graft failure following transplantation into the subretinal space in nonhuman primates. *Invest Ophthalmol vis Sci.* 2018;59(3):1374-1383.
11. Chao JR, Lamba DA, Klesert TR, et al. Transplantation of human embryonic stem cell-derived retinal cells into the subretinal space of a non human primate. *Transl vis Sci Technol.* 2017;6(3):4.
12. Aboualizadeh E, Phillips MJ, McGregor JE, et al. Imaging transplanted photoreceptors in living nonhuman primates with single cell resolution. *Stem Cell Reports.* 2020;15(2):482-497.
13. Moshiri A, Chen R, Kim S, et al. A nonhuman primate model of inherited retinal disease. *J Clin Investig.* 2019;129(2):863-874.
14. McBride JL, Neuringer M, Ferguson B, et al. Discovery of a CLN7 model of Batten disease in non-human primates. *Neurobiol Dis.* 2018;119:65-78.
15. Peterson SM, McGill TJ, Puthussery T, et al. Bardet-Biedl syndrome in rhesus macaques: a nonhuman primate model of retinitis pigmentosa. *Exp Eye Res.* 2019;189:107825.
16. Wu K-C, Lv J-N, Yang H, et al. Nonhuman primate model of oculocutaneous albinism with TYR and OCA2 mutations. *Research (Wash D C).* 2020;2020:1658678.
17. McGill TJ, Stoddard J, Renner LM, et al. Allogeneic iPSC-derived RPE cell graft failure following transplantation into the subretinal space in non-human primates. *Invest Ophthalmol vis Sci.* 2018;59(3):1374-1383.
18. Osakada F, Ikeda H, Mandai M, et al. Toward the generation of rod and cone photoreceptors from mouse, monkey and human embryonic stem cells. *Nat Biotechnol.* 2008;26(2):215-224.
19. D'Souza SS, Maufort J, Kumar A, et al. GSK3β inhibition promotes efficient myeloid and lymphoid hematopoiesis from non-human primate-induced pluripotent stem cells. *Stem Cell Reports.* 2016;6(2):243-256.
20. Hong SG, Yada RC, Choi K, et al. Rhesus iPSC safe harbor gene-editing platform for stable expression of transgenes in differentiated cells of all germ layers. *Mol Ther.* 2017;25(1):44-53.

21. Lin Y, Liu H, Klein M, et al. Efficient differentiation of cardiomyocytes and generation of calcium-sensor reporter lines from nonhuman primate iPSCs. *Sci Rep.* 2018;8(1):5907.

22. Stauske M, Rodriguez Polo I, Haas W, et al. Non-human primate iPSC generation, cultivation, and cardiac differentiation under chemically defined conditions. *Cells.* 2020;9(6):1349.

23. Kuwahara A, Ozone C, Nakano T, Saito K, Eiraku M, Sasai Y. Generation of a ciliary margin-like stem cell niche from self-organizing human retinal tissue. *Nat Commun.* 2015;6(1):6286.

24. Meyer JS, Howden SE, Wallace KA, et al. Optic vesicle-like structures derived from human pluripotent stem cells facilitate a customized approach to retinal disease treatment. *Stem Cells.* 2011;29(8):1206-1218.

25. Eiraku M, Takata N, Ishibashi H, et al. Self-organizing optic-cup morphogenesis in three dimensional culture. *Nature.* 2011;472(7341):51-56.

26. Sosa E, Kim R, Rojas EJ, et al. An integration-free, virus-free rhesus macaque induced pluripotent stem cell line (riPSC89) from embryonic fibroblasts. *Stem Cell Res.* 2016;17(2):444-447.

27. Sosa E, Kim R, Rojas EJ, et al. An integration-free, virus-free rhesus macaque induced pluripotent stem cell line (riPSC90) from embryonic fibroblasts. *Stem Cell Res.* 2017;21:5-8.

28. Capowski EE, Samimi K, Mayerl SJ, et al. Reproducibility and staging of 3D human retinal organoids across multiple pluripotent stem cell lines. *Development.* 2019;146(1):dev171686.

29. Zhong X, Gutierrez C, Xue T, et al. Generation of three-dimensional retinal tissue with functional photoreceptors from human iPSCs. *Nat Commun.* 2014;5(1):4047.

30. Brzezinski JA IV, Lamba DA, Reh TA. Blimp1 controls photoreceptor versus bipolar cell fate choice during retinal development. *Development.* 2010;137(4):619-629.

31. Silk J, Short J, Roberts J, Kusnitz J. Gestation length in rhesus macaques (Macaca mulatta). *Int J Primatol.* 1993;14(1):95-104.

32. American College of Obstetricians and Gynecologists. ACOG committee opinion No 579: definition of term pregnancy. *Obstet Gynecol.* 2013;122(5):1139-1140.

SUPPORTING INFORMATION

Additional supporting information may be found in the online version of the article at the publisher's website.